npj | parkinson's disease

Article

Published in partnership with the Parkinson's Foundation

https://doi.org/10.1038/s41531-025-00944-x

Cortical microstructural abnormalities in dementia with Lewy bodies and their associations with Alzheimer's disease copathologies

Elijah Mak[1,2] ✉, Robert I. Reid[1,3], Scott A. Przybelski[4], Angela M. Fought[4], Timothy G. Lesnick[4], Christopher G. Schwarz[1], Matthew L. Senjem[1,3], Sheelakumari Raghavan[1], Prashanthi Vemuri[1], Clifford R. Jack Jr[1], Hoon Ki Min[1], Manoj K. Jain[5], Toji Miyagawa[6], Leah K. Forsberg[6], Julie A. Fields[7], Rodolfo Savica[6], Jonathan Graff-Radford[6], David T. Jones[6], Hugo Botha[6], Erik K. St. Louis[6,7,8], David S. Knopman[6], Vijay K. Ramanan[6], Dennis W. Dickson[9], Neill R. Graff-Radford[10], Gregory S. Day[10], Tanis J. Ferman[11], Ronald C. Petersen[4,6], Val J. Lowe[1], Bradley F. Boeve[6], John T. O'Brien[2] & Kejal Kantarci[1]

Dementia with Lewy bodies (DLB) frequently coexists with Alzheimer's disease pathology, yet the pattern of cortical microstructural injury and its relationship with amyloid, tau, and cerebrovascular pathologies remains unclear. We applied neurite orientation dispersion and density imaging (NODDI) to assess cortical microstructural integrity in 57 individuals within the DLB spectrum and 57 age- and sex-matched cognitively unimpaired controls by quantifying mean diffusivity (MD), tissue-weighted neurite density index (tNDI), orientation dispersion index (ODI), and free water fraction (FWF). Amyloid and tau levels were measured using PiB and Flortaucipir PET imaging. Compared to controls, DLB exhibited increased MD and FWF, reduced tNDI across multiple regions, and focal ODI reductions in the occipital cortex. Structural equation modeling revealed that APOE genotype influenced amyloid levels, which elevated tau, leading to microstructural injury. These findings highlight the role of AD pathology in DLB neurodegeneration, advocating for multi-target therapeutic approaches addressing both AD and DLB-specific pathologies.

Dementia with Lewy bodies (DLB) is the second most common cause of neurodegenerative dementia[1], with core clinical features including visual hallucinations, parkinsonism, cognitive fluctuations, and REM sleep behavior disorder[2]. While the defining pathology of DLB is the aggregation of α-synuclein forming Lewy bodies and neurites, co-existing Alzheimer's disease (AD) neuropathologic changes, including amyloid plaques and neurofibrillary tangles (NFT), are reported in over 70% of cases[3].

Both amyloid-β and tau have been demonstrated to influence clinical phenotype, disease progression, prognosis, and survival[4–6]. The apolipoprotein E ε4 allele (APOE4), a well-established genetic risk factor for AD, has also been implicated in DLB pathogenesis, potentially influencing both α-synuclein aggregation and AD copathology[7,8]. Despite the known involvement of amyloid-β, tau, and APOE4 in DLB, the precise mechanisms by which these factors influence its progression remain unclear. Post-mortem studies demonstrate that DLB patients with high Braak NFT tau stages

[1]Department of Radiology, Mayo Clinic, Rochester, MN, USA. [2]Department of Psychiatry, University of Cambridge, Cambridge, United Kingdom. [3]Department of Information Technology, Mayo Clinic, Rochester, MN, USA. [4]Department of Quantitative Health Sciences, Mayo Clinic, Rochester, MN, USA. [5]Department of Radiology, Mayo Clinic, Jacksonville, FL, USA. [6]Department of Neurology, Mayo Clinic, Rochester, MN, USA. [7]Department of Psychiatry and Psychology, Mayo Clinic, Rochester, MN, USA. [8]Center for Sleep Medicine, Division of Pulmonary and Critical Care Medicine, Department of Medicine, Mayo Clinic, Rochester, MN, USA. [9]Laboratory of Medicine and Pathology, Mayo Clinic in Florida, Jacksonville, FL, USA. [10]Department of Neurology, Mayo Clinic in Florida, Jacksonville, FL, USA. [11]Department of Psychiatry and Psychology, Mayo Clinic in Florida, Jacksonville, FL, USA.
✉e-mail: mak.elijah@mayo.edu

exhibit more severe atrophy in stereotypical AD regions, such as the temporoparietal cortices, hippocampus, and amygdala[9,10]. These findings have since been corroborated by in vivo PET imaging studies examining the associations between AD biomarkers and the extent of neurodegenerative changes, typically measured by brain atrophy on structural MRI[11–15]. However, the sensitivity of conventional structural MRI biomarkers to early AD-related changes may be limited, as macrostructural gray matter atrophy typically represents the end-stage of a cascade of neurodegenerative cellular events, such as early morphological alterations in dendritic spines and synaptic dysfunction prior to cell death[16].

Diffusion MRI (dMRI) is a non-invasive MRI technique that is sensitive to subtle changes in the integrity of neuronal structures[17]. Whereas dMRI in DLB has traditionally been applied to evaluate the integrity of white matter tracts[18–23], there has been a paradigm shift with the growing recognition that dMRI could be a sensitive technique to probe gray matter diffusion changes that may reflect early synaptic loss and associated breakdown of neuronal cytoarchitectural within the cortex[24,25]. Previous studies using single-shell DTI have demonstrated a disease-related increase in gray matter mean diffusivity (MD) in DLB[24], presymptomatic familial mutation carriers of AD[26], MCI[27], and sporadic AD[28], highlighting the potential that gray matter MD may serve as a non-invasive, accessible biomarker of early microstructural alterations predating macroscale neuronal loss. However, the interpretations of gray matter MD remain controversial for several reasons. First, partial volume effects (PVE) of contamination from surrounding CSF would inflate MD values, thereby leading to a conflation of disease-related effects, particularly in studies of neurodegenerative conditions where profound atrophy may already be present[24,28]. Second, in contrast to the more coherently oriented axons along the white matter tracts, the complex cytoarchitecture of cortical gray matter —with its heterogeneous mix of cell types and crossing fibers—poses inherent challenges in accurately modeling diffusion. Third, the cellular mechanisms underlying elevated MD remain ambiguous since increased extracellular space secondary to atrophy could also drive MD elevations without neuritic degeneration[29].

Neurite Orientation Dispersion and Density Imaging (NODDI) is an advanced biophysical multi-shell DWI acquisition model that can differentiate signal contributions from intracellular and extracellular tissue compartments, providing quantitative estimates of neurite density (NDI), orientation dispersion (ODI) and free water fraction (FWF)[30]. NODDI offers several advantages over conventional DTI techniques in interpreting gray matter alterations. Firstly, NODDI employs a multi-compartment modeling approach that distinguishes between intracellular, extracellular, and CSF compartments, allowing for the quantification of the CSF-fraction of the diffusion signal and minimizing contamination and partial volume effects[31]. Secondly, the fiber orientation dispersion estimates, representing the angular variation of the diffusion signal, are better suited to characterize the complex fiber architecture of the heterogeneous neuronal structure comprising different cell types with dispersed orientations[32]. Finally, the compartment-specific quantification of NODDI provides biologically plausible estimates of neurite density from the intracellular space, rather than relying on non-specific markers conflating both intra- and extracellular sources. Indeed, several studies using NODDI in the gray matter have demonstrated relevant neurobiological changes in various contexts, including normal aging[33–35], accelerated age-related ODI decreases among cognitively normal APOE4 carriers[36], and widespread loss of NDI and ODI in young-onset AD[37], MAPT mutation carriers[38], and patients with primary tauopathies[39]. Additionally, free water mapping has shown promise in detecting subtle tissue alterations in neurodegenerative conditions[40–42]. In AD, elevated free water in white matter has been associated with cognitive decline and may serve as a marker of early pathological changes[41].

The present study aims to address several key questions regarding gray matter microstructural changes in the DLB spectrum and their relationship to AD copathologies. First, we seek to characterize the regional patterns of gray matter microstructural alterations in DLB as seen on conventional DTI and advanced NODDI metrics, comparing these to cognitively normal controls. Second, we aim to characterize the multivariate pathways of APOE4 genotype, cerebrovascular disease, and AD biomarkers associated with gray matter neurite abnormalities in the DLB spectrum. Third, we will explore the potential clinical relevance of these neurite alterations by examining their associations with disease severity and the hallmark clinical features of DLB.

Table 1 | Sample characteristics of matched CU controls versus DLB spectrum with the mean (SD) listed for the continuous variables and count (%) for the categorical variables

	CU $n = 57$	DLB Spectrum $n = 57$	*P* value
Age, yrs	69.2 (8.6)	69.2 (8.5)	0.25
Males, no. (%)	50 (88%)	50 (88%)	1.00
APOE ε4 carrier, no. (%)	13 (27%)	22 (42%)	0.11
Education, yrs	15.6 (2.4)	15.7 (2.9)	0.81
MMSE	29.1 (0.8)	23.9 (4.8)	<0.001
CDR-SB	0.0 (0.0)	5.0 (3.5)	<0.001
Meta Tau (SUVr)	1.19 (0.09)	1.27 (0.19)	0.006
Abnormal Meta Tau, no. (%)	13 (23%)	25 (44%)	0.011
Meta PiB (SUVr)	1.50 (0.31)	1.69 (0.43)	0.010
Abnormal Meta PiB, no. (%)	18 (32%)	29 (51%)	0.034
WMH (% of TIV)	0.56 (0.49)	0.74 (0.68)	0.10
Visual hallucinations, no. (%)	NA	20 (35%)	
Fluctuations, no. (%)	NA	33 (58%)	
Parkinsonism, no. (%)	NA	52 (91%)	
RBD, no. (%)	NA	51 (89%)	
UPDRS-III	NA	21.0 (14.5)	

P values for differences between groups are derived from a conditional logistic model, except for MMSE and CDR-SB, which were analyzed using an exact conditional logistic model. APOE ε4 carrier status is defined as the presence of at least one ε4 allele. *APOE* apolipoprotein E, CDR-SB clinical dementia rating, sum-of-boxes, *CU* cognitively unimpaired, *DLB* dementia with Lewy bodies, *MMSE* mini-mental state examination, *RBD* REM sleep behavior disorder, *WMH* white matter hyperintensities, *TIV* total intracranial volume, *UPDRS-III* unified Parkinson's disease rating scale, *SUVr* standardized uptake value ratio. Note: APOE data were missing in 8 CU and 4 DLB.

Results

Sample characteristics

Participant characteristics are summarized in Table 1. By design, the DLB spectrum and CU groups were comparable in age. The groups were similar with education years, and APOE4 carrier status. As expected, the DLB spectrum group had statistically significantly lower MMSE scores than the CU group. Cortical Flortaucipir and PiB SUVr values were elevated in the DLB spectrum compared to the CU controls. While the percentage of WMH was higher in the DLB spectrum group, this difference did not reach statistical significance. Regarding core clinical DLB features, 35% of patients with DLB spectrum had visual hallucinations, 58% had cognitive fluctuations, 91% had parkinsonism, and 89% had RBD (of whom 23.5% were confirmed by polysomnography).

Group differences in gray matter microstructure between the DLB spectrum and CU groups

Figure 1 depicts topographical patterns of group differences between the DLB spectrum patients and CU participants. These results highlight a pattern of widespread microstructural injury in DLB, with particularly pronounced effects in temporal, limbic, and parietal regions for MD, tNDI, FWF, and more localized effects in posterior brain regions for ODI. Compared to CU participants, the DLB spectrum group showed significantly

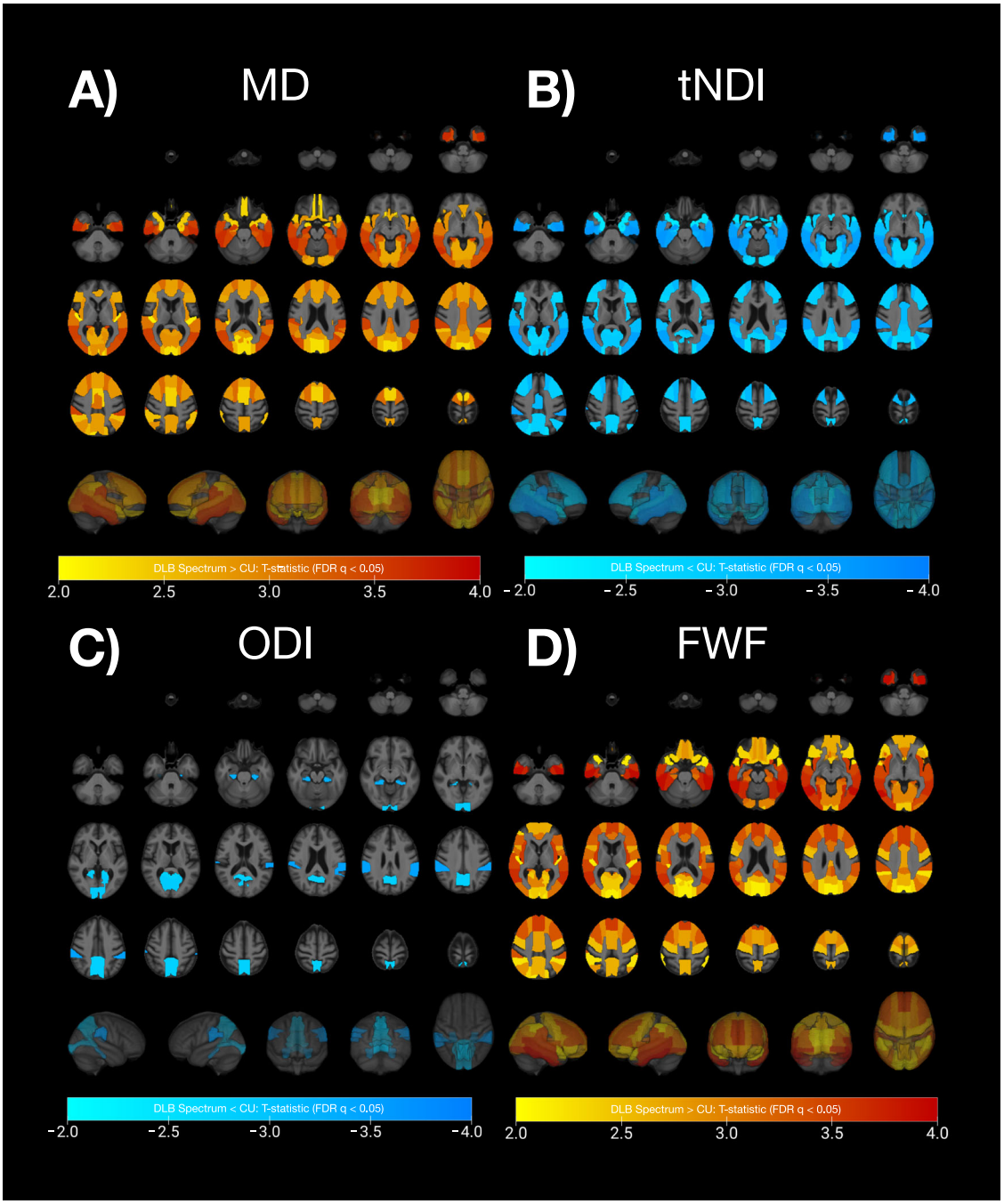

Fig. 1 | Topographic distributions of GM microstructural injury in DLB spectrum relative to matched CU individuals. Pairwise group differences in (**a**) regional MD, (**b**) tNDI, (**c**) ODI, and (**d**) FWF were examined using conditional logistic regression models to account for the 1:1 matching between groups. T-statistics from the significant comparisons after adjusting for FDR are depicted on both volumetric templates and 3D glass brain renderings. In the DLB spectrum group, significantly elevated MD and FWF was accompanied by decreased tNDI across widespread GM regions, while reductions in ODI were more focal and preferentially localized to posterior-occipital brain regions. CU cognitively unimpaired, DLB dementia with Lewy bodies, FDR false discovery rate, GM gray matter, MD mean diffusivity. ODI orientation dispersion index, tNDI tissue-weighted neurite density index, FWF free water fraction.

elevated MD across 74.4% of gray matter ROIs. The most pronounced MD elevations were observed in the inferior temporal gyrus ($Z = 3.66$), hippocampus ($Z = 3.51$), middle temporal gyrus ($Z = 3.49$), supramarginal gyrus ($Z = 3.48$), and fusiform gyrus ($Z = 3.47$). The DLB spectrum group showed reduced tNDI across 58.1% of ROIs, predominantly in limbic, temporal, occipital, parietal, and frontal lobes. The largest tNDI reductions were found in the middle occipital gyrus ($Z = -3.49$), hippocampus ($Z = -3.46$), inferior temporal gyrus ($Z = -3.29$), supramarginal gyrus ($Z = -3.27$), inferior occipital gyrus ($Z = -3.05$), and middle temporal gyrus ($Z = -3.03$). ODI reductions were more localized, affecting 9.3% of ROIs, primarily in posterior parietal, occipital, and limbic regions, such as the calcarine cortex ($Z = -3.28$), parahippocampal gyrus ($Z = -3.04$), precuneus ($Z = -3.02$), and supramarginal gyrus ($Z = -2.98$). There were also widespread increases in FWF across multiple brain regions in the DLB spectrum group compared to the CU participants (83.7% of gray matter ROIs), with particularly strong effects in the inferior temporal gyrus ($Z = 3.90$), fusiform ($Z = 3.71$), middle temporal lobe ($Z = 3.6$), inferior occipital gyrus ($Z = 3.57$) and insula ($Z = 3.55$).

We observed substantial overlap in the topographical patterns of group differences for MD, tNDI, and FWF. To quantify these spatial relationships,

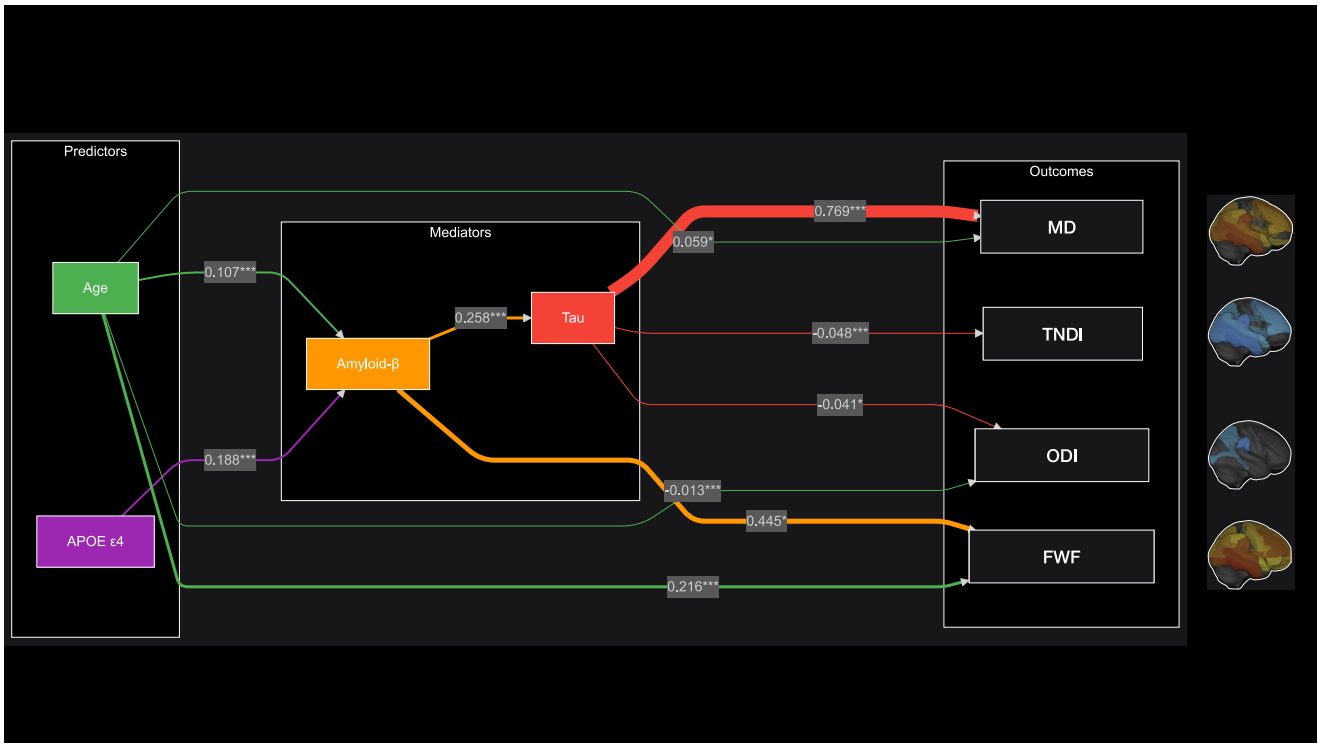

Fig. 2 | Structural equation modeling of pathological cascades associated with microstructural injury in DLB. The diagram shows significant direct effects ($p < 0.05$) between age, APOE ε4 genotype, AD biomarkers (amyloid-β and tau), and composite measures of gray matter microstructure (MD, tNDI, ODI, and FWF) in the DLB spectrum. Pathways are color-coded by their origin: age (green), APOE (purple), amyloid-β (orange), and tau (red). Line thickness is proportional to the magnitude of the standardized coefficient, with values and significance levels shown (***$p < 0.001$, **$p < 0.01$, *$p < 0.05$). Variables were transformed for analysis: amyloid-β and tau were log-transformed, age was measured in decades, and mean diffusivity was scaled by 100. The model reveals both direct pathways (e.g., tau → MD) and indirect pathways (e.g., APOE → amyloid-β → tau) contributing to microstructural changes. To interpret the SEM findings within the context of anatomical patterns, the topography of each composite GM microstructure is provided next to the DTI and NODDI nodes (FDR $q < 0.05$ from pairwise group comparisons between DLB spectrum and CU controls). AD Alzheimer's disease, APOE apolipoprotein E, CU cognitively unimpaired, DLB dementia with Lewy bodies, FWF free water fraction, FDR false discovery rate, GM gray matter, MD mean diffusivity, ODI orientation dispersion index, *tNDI* tissue-weighted neurite density index, SEM structural equation modeling.

Dice coefficients were computed between the binarized maps of significant group differences. The highest concordance was found between MD and tNDI (Dice = 0.88), and between MD and FWF (Dice = 0.88), followed by tNDI and FWF (Dice = 0.75). In contrast, the topography of ODI reductions showed minimal concordance with the other metrics, as evidenced by markedly lower Dice coefficients: ODI-MD (Dice = 0.22), ODI-tNDI (Dice = 0.28), and ODI-FWF (Dice = 0.20).

To assess the independence of microstructural changes from macrostructural atrophy, we conducted a sensitivity analysis by including regional gray matter volume (expressed as a percentage of total intracranial volume) as a covariate in our statistical models. This adjustment substantially reduced the spatial extent of group differences in microstructural metrics: the proportion of gray matter regions showing significant microstructural alterations decreased from 74.4 to 25.6% for MD, from 58.1 to 14% for tNDI, and from 83.7 to 55.8% for FWF. Notably, ODI reductions were no longer statistically significant after controlling for regional gray matter volumes.

Structural equation modeling

The fit indices for the SEMs were good, with CFI = 1.00 and RMSEA <0.05 across the models for the composite MD, tNDI, and ODI ROIs, providing support for the hypothesized theoretical pathways. For the FWF model, fit indices were acceptable with CFI = 0.96, though slightly below optimal thresholds for TLI (0.88), and RMSEA = 0.12. Significant direct and indirect effects, along with standardized parameter estimates and coefficients, are depicted in Fig. 2 and tabulated in Table 2. WMH did not significantly relate to the composite diffusion metrics and were therefore not included in the final parsimonious models after backward elimination.

Both exogenous predictors, age (β = 0.107, $p < 0.001$) and APOE ε4 genotype (β = 0.188, $p < 0.001$) had significant direct effects on amyloid accumulation ($R^2 = 0.330$), Amyloid, in turn, had direct effects on increased tau deposition (β = 0.258, $p < 0.001$) and increased FWF (β = 0.445, $p = 0.027$, $R^2 = 0.392$). Tau showed significant direct effects on (i) higher MD (β = 0.769, $p < 0.001$, $R^2 = 0.364$), lower tNDI (β = −0.048, $p < 0.001$, $R^2 = 0.255$), and lower ODI (β = -0.041, $p = 0.029$, $R^2 = 0.373$). Tau showed no significant direct effect on FWF. In addition, age demonstrated significant direct effects on elevated MD (β = 0.059, $p = 0.035$) and lower ODI (β = -0.013, $p < 0.001$), elevated FWF (β = 0.216, $p < 0.001$) but not tNDI.

Both exogenous predictors of older age (β = 0.028, $p = 0.011$) and APOE ε4 genotype (β = 0.048, $p = 0.011$) had indirect effects on increasing tau through amyloid, as well as smaller indirect effects on MD and tNDI, mediated through amyloid and tau pathways: Age → Amyloid → Tau → MD (β = 0.021, $p = 0.029$); Age → Amyloid → Tau → tNDI (β = −0.001, $p = 0.029$); APOE ε4 → Amyloid → Tau → MD (β = 0.037, $p = 0.029$; APOE ε4 → Amyloid → Tau → tNDI (β = −0.002, $p = 0.029$). Although amyloid did not directly influence gray matter microstructural injury, it had indirect effects through tau on elevated MD (β = 0.198, $p = 0.005$) and reduced tNDI (β = −0.012, $p = 0.005$). In contrast, FWF showed a distinct pattern of indirect effects that did not reach statistical significance nor involve tau: (i) Age → Amyloid → FWF (β = 0.048, $p = 0.061$) and (ii) APOE ε4 → Amyloid → FWF (β = 0.084, $p = 0.061$).

Table 2 | Structural equation modeling results showing the direct, indirect, and total effects of age, APOE genotype, amyloid-β, and tau on GM microstructural injury in DLB spectrum

Type of effects	Paths	Coefficient (SE)	*P* value
Direct Effects	Age → PiB	0.107 (0.030)	<0.001
	Apoe → PiB	0.188 (0.054)	<0.001
	PiB → Tau	0.258 (0.070)	<0.001
	Age → MD	0.059 (0.028)	0.035
	Tau → MD	0.769 (0.181)	<0.001
	Tau → TNDI	-0.048 (0.011)	<0.001
	Age → ODI	-0.013 (0.003)	<0.001
	Tau → ODI	-0.041 (0.019)	0.029
	Age → FWF	0.216 (0.055)	<0.001
	PiB → FWF	0.445 (0.201)	0.027
Indirect Effects	Age → PiB → Tau	0.028 (0.011)	0.011
	Apoe → PiB → Tau	0.048 (0.019)	0.011
	Age → PiB → Tau → MD	0.021 (0.010)	0.029
	Apoe → PiB → Tau → MD	0.037 (0.017)	0.029
	PiB → Tau → MD	0.198 (0.071)	0.005
	Age → PiB → Tau → TNDI	-0.001 (0.001)	0.029
	Apoe → PiB → Tau → TNDI	-0.002 (0.001)	0.029
	PiB → Tau → TNDI	-0.012 (0.004)	0.005
	Age → PiB → Tau → ODI	-0.001 (0.001)	0.098
	Apoe → PiB → Tau → ODI	-0.002 (0.001)	0.098
	PiB → Tau → ODI	-0.011 (0.006)	0.061
	Age → PiB → FWF	0.048 (0.025)	0.061
	Apoe → PiB → FWF	0.084 (0.045)	0.061
Total Effects	Age → MD	0.080 (0.028)	0.004
	Age → ODI	-0.014 (0.003)	<0.001
	Age → FWF	0.264 (0.052)	<0.001

Amyloid-β and tau were log-transformed to reduce their positive skew, and age was in decades. MD was scaled by 100 to ease model fitting. FWF is 100*FWF and was log-transformed. The table presents the unstandardized coefficients, SE, and *p* values for each pathway in the SEMs. *APOE* apolipoprotein E, *DLB* dementia with Lewy bodies, *FWF* free water fraction, *GM* gray matter, *MD* mean diffusivity, *tNDI* tissue-weighted neurite density index, *ODI* orientation dispersion index, *SE* standard errors, *SEM* structural equation modeling.

Total effects. When considering the combined impact of all direct and indirect pathways, age emerged as a significant predictor across multiple measures of gray matter microstructure. The total effects analysis revealed that older age was independently associated with elevated MD (β = 0.080, $p = 0.004$), lower ODI (β = -0.014, $p < 0.001$), and higher FWF (β = 0.264, $p < 0.001$).

Regional associations of amyloid, tau, and WMH with gray matter microstructure

Multivariable regression analyses revealed significant associations between tau deposition and regional gray matter microstructural injury in the DLB spectrum group, after accounting for age, APOE genotype, amyloid-β, regional gray matter volumes, and WMH and adjusting for multiple comparisons with FDR. Specifically, a higher tau burden was associated with elevated MD in 26% of all ROIs, predominantly involving the temporal and limbic lobes. Higher tau deposition was also associated with lower tNDI (14% of all gray matter ROIs). The middle temporal gyrus exhibited the most pronounced effects of tau on both MD (T-statistic = 3.9) and tNDI (T-statistic = −4.0, Fig. 3). In contrast, no statistically significant correlations were found between tau and regional ODI after FDR correction. Furthermore, amyloid-β levels and WMH did not significantly relate to gray matter microstructural metrics in the DLB spectrum (Supplementary Fig. 1), although increased hippocampal FWF was associated with greater WMH burden (T-statistic = 4.4, FDR $q = 0.002$). No significant associations were observed between tau, amyloid-β deposition, or WMH and diffusion measures of gray matter microstructure in the CU group (Supplementary Fig. 2). Supplemental analyses of region-by-region correlation between tau PET with DTI and NODDI metrics revealed broadly similar patterns of correlations in the DLB spectrum group (Supplementary Fig. 3).

Associations of gray matter microstructure with clinical features

We conducted exploratory analyses within the DLB spectrum group to examine associations between clinical features and composite ROIs of MD and NODDI metrics (derived from FDR-adjusted group differences between DLB spectrum and CU controls). After adjusting for age, we found no significant associations between UPDRS-III scores or CDR-SB and three metrics: MD, tNDI, and ODI. However, FWF showed a weak positive correlation with UPDRS-III scores ($R = 0.294$, $p = 0.029$, Fig. 4). When comparing DLB spectrum patients with and without core clinical features (visual hallucinations, fluctuations, and parkinsonism), we found no significant group differences in any composite ROIs. However, patients with RBD showed significantly higher ODI values compared to those without RBD ($p = 0.016$, Supplementary Fig. 4).

Discussion

We characterized the in vivo regional gray matter patterns of neurite and dendritic abnormalities in the continuum of prodromal and probable DLB and evaluated their associations with co-existing AD PET biomarkers and cerebrovascular burden. First, the DLB spectrum group showed extensive abnormalities in MD, tNDI, and FWF across multiple brain regions largely independent of macrostructural atrophy, while ODI reductions were more focal and primarily in the occipital cortex. Second, our SEMs disentangled the complex etiology of gray matter microstructural injury in DLB by proposing a model that aligned with the classical AD pathogenic cascade (APOE → amyloid-β → Tau → Neurodegeneration), which in part explained the NODDI findings. WMHs did not significantly relate to the observed patterns of gray matter microstructural injury. Our findings advocate for the further assessment of anti-AD interventions within a multi-pronged disease-modifying strategy for DLB and underscore the potential of NODDI as a valuable measure of neurodegeneration driven by co-existing AD pathology in DLB.

As hypothesized, the DLB spectrum group exhibited widespread microstructural alterations compared to controls, characterized by elevated MD, reduced tNDI, and increased FWF across hemispheric cortices, along with localized reductions of ODI in parietal-occipital cortices. While our study comprehensively characterized regional gray matter microstructure along the DLB spectrum, the diffuse topography and magnitude of neurite abnormalities in individuals within the DLB spectrum corroborate and extend the growing literature demonstrating robust cortical neurite abnormalities in other neurodegenerative diseases, including patients with young-onset AD, and other primary tauopathies[31,36–39,43,44]. To the extent that diffusion MRI may reflect subtle changes in the neuropil of the gray matter and, therefore, synaptic health[39], the widespread loss of tNDI and increased FWF is aligned with the extensive synaptic dysfunction that characterizes DLB[45,46]. The concurrent findings of elevated MD, reduced tNDI, and increased FWF suggest multiple complementary aspects of tissue degradation, such as loss of neurite density and compromised cellular

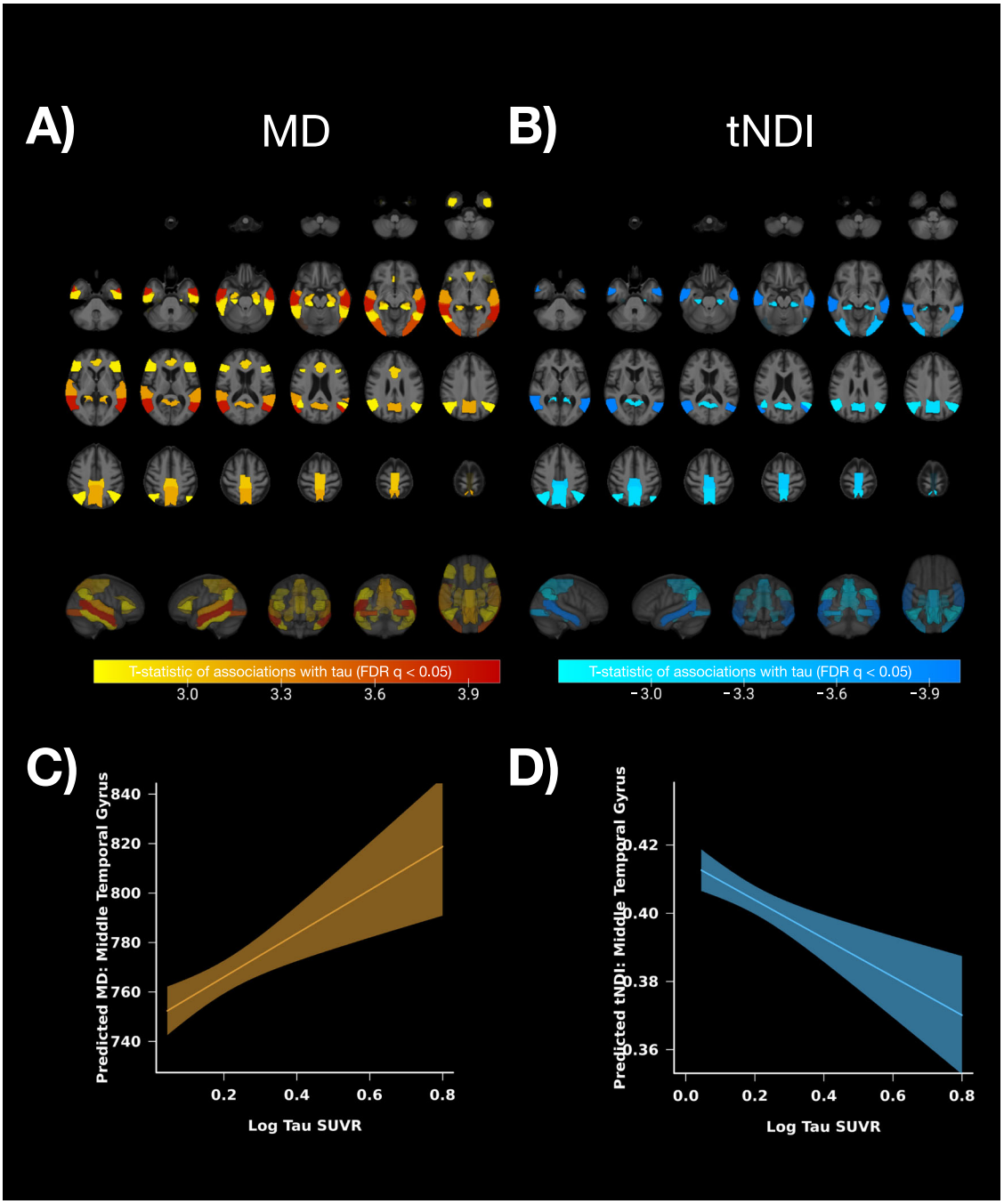

Fig. 3 | Regional associations between tau and GM microstructure integrity in DLB spectrum. A T-statistics map showing significant associations between tau and MD after FDR correction. Yellow-red colors indicate positive associations. **B** T-statistics map showing significant associations between tau and tNDI after FDR correction. Blue colors indicate negative associations. **C** Scatter plot showing the positive relationship between log tau SUVR and predicted MD values in the middle temporal gyrus, with a 95% confidence interval shown in brown shading. **D** Scatter plot showing the negative relationship between log tau SUVR and predicted tNDI values in the middle temporal gyrus, with a 95% confidence interval shown in blue shading. All regression models were adjusted for age, APOE genotype, amyloid-β, gray matter volume (expressed as a % of TIV), and WMH (expressed as a % of TIV). APOE apolipoprotein E, DLB dementia with Lewy bodies, FDR false discovery rate, GM gray matter, MD mean diffusivity, SUVR standardized uptake value ratio, tNDI tissue-weighted neurite density index, TIV total intracranial volume, WMH white matter hyperintensities.

architecture, increased overall diffusivity due to the breakdown of cellular barriers, while increased FWF suggests an expansion of the extracellular space, potentially reflecting edema or neuroinflammatory processes.

The selective preservation of neurite microstructure in the primary sensory cortex is substantiated by multiple research studies[47] and is in keeping with previous reports of relative preservation of metabolic function[48], white matter pathways[19], and functional connectivity[49] along the DLB spectrum.

Previous studies have demonstrated that NODDI is sensitive to disease-related abnormalities over and beyond that of macrostructural neurodegeneration[37,39]. Our supplemental analyses broadly supported this notion, as DLB spectrum individuals showed elevated MD, reduced tNDI, and increased FWF in multiple regions, even after controlling for regional gray matter atrophy. The persistence of significant differences in some regions after this correction underscores that diffusion metrics can capture aspects of tissue integrity not fully reflected by volumetric measures alone[28].

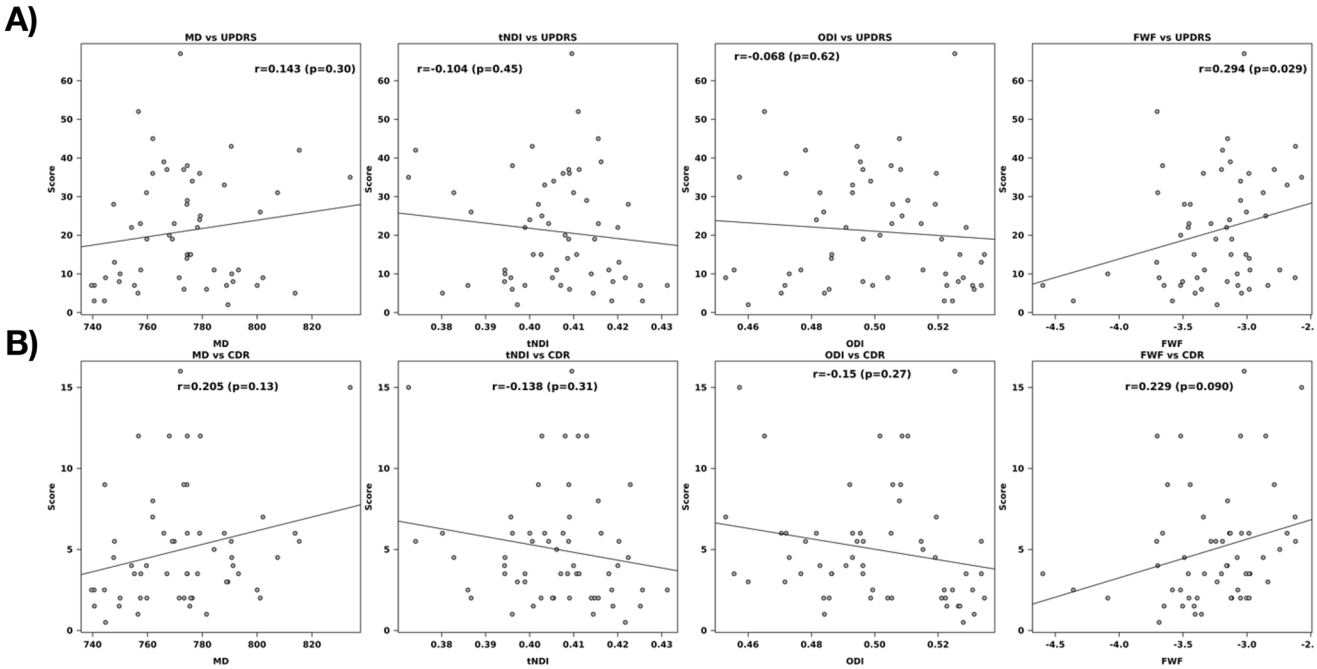

Fig. 4 | Associations between gray matter microstructure metrices and clinical measures in dementia with Lewy bodies. Scatterplots rerpesent age-adjusted correlations between composite gray matter microstructural metrics and clinical measures in the DLB spectrum group. **A** Associations with motor severity (**B**) Associations with global cognitive impairment. CDR-SB Clinical Dementia Rating-Sum of Boxes, DLB Dementia with Lewy Bodies, GM Gray Matter, MD Mean Diffusivity, tNDI tissue-weighted Neurite Density Index, ODI Orientation Dispersion Index, FWF Free Water Fraction, ROI Region of Interest, UPDRS-III Unified Parkinson's Disease Rating Scale Part III.

However, the substantial reduction in the number of regions showing significant microstructural differences after correcting for gray matter volume warrants careful consideration. This reduction suggests a strong relationship between microstructural changes and atrophy in DLB, with volume correction accounting for a large portion of the variance in diffusion metrics initially attributed to disease effects. Additionally, this reduction might partly reflect the mitigation of partial volume effects, which have been documented by previous studies[28]. In neurodegenerative conditions like DLB where atrophy is present, the increased proportion of CSF in a voxel (i.e., 2 mm isotropic in the present study) would theoretically inflate MD values and decrease NDI values. These findings indicate that while macrostructural and microstructural changes are closely related in DLB, they are not entirely redundant. Longitudinal studies are imperative to elucidate the temporal relationship between macrostructural atrophy and neurite alterations in DLB. Such studies could reveal whether microstructural changes precede macroscopic atrophy in specific brain regions, potentially validating diffusion MRI metrics as early biomarkers of neurodegeneration before significant atrophy becomes detectable.

In contrast to the diffuse patterns of MD, tNDI, and FWF alterations, the selective ODI reductions in posterior parietal-occipital regions merit further discussion. Decreased ODI is typically considered to reflect reduced complexity of dendritic processes[32], and we have previously demonstrated its close coupling with lower synaptic density using UCB-J PET imaging[39]. Intriguingly, these ODI reductions coincided with the topography of hypometabolic and perfusion deficits that we have previously reported in DLB patients[50]. This spatial overlap raises the possibility that compromised dendritic complexity in the occipital lobe could represent a microstructural "fingerprint" underlying the neuronal deficits detected using arterial spin labeling (ASL) and fluorodeoxyglucose (FDG)-PET neuroimaging in DLB. Collectively, these findings point to a predilection for occipital lobe involvement that could be associated with α-synuclein-related synaptic injury, but also be associated with the atypical temporoparietal-occipital distribution of tau PET uptake observed in our prior studies in PDD and DLB[51,52]. Corroborating this notion, autopsy studies of clinically diagnosed probable DLB patients have revealed the greatest burden of hyperphosphorylated tau pathology in the occipital lobes[5]. Although direct evidence linking ODI changes with perfusion or metabolic deficits is currently lacking in DLB or other dementias, our hypothesis is further supported by previous studies showing tangential associations between NODDI and resting-state functional connectivity[53]. Moreover, higher ODI values in the default mode and visual association networks were associated with increased local functional connectivity[54]. Future multimodal studies are needed to evaluate the interaction between NODDI and functional biomarkers and to delineate how perturbations in this structure–function relationship could modulate disease trajectory or clinical manifestations in DLB.

Through our simultaneous analyses of pairwise group differences in diffusion metrics and comparison of Dice coefficients, we observed substantial spatial overlap among several measures. The highest concordance was found between MD and tNDI (Dice = 0.88), and between MD and FWF (Dice = 0.88), followed by tNDI and FWF (Dice = 0.75). In contrast, ODI showed minimal spatial concordance with other metrics (ODI-MD: 0.22, ODI-tNDI: 0.28, ODI-FWF: 0.20). Considering recent data showing a strong correlation between NDI and MD values ($R = 0.97$)[55], these overlapping patterns may suggest shared underlying mechanisms that collectively contribute to the degeneration of neuronal architecture in the spectrum of DLB. These mechanisms could include, but are not limited to, spinodendritic degeneration[56], axonal and synaptic loss, and neuronal death —all of which would be expected to result in the breakdown of cellular barriers and manifest as increased overall diffusion magnitude (elevated MD) and reduced neurite density (lower tDI) and increased free water diffusivity (higher FWF). Playing the devil's advocate, one might question whether the striking topological similarities between MD, tNDI, and FWF imply redundancy in multi-shell NODDI acquisitions. However, we contend that these overlapping patterns provide valuable mechanistic insights when interpreted together. The high spatial concordance between MD and tNDI suggests that elevated MD in DLB primarily reflects neurite loss. Similarly, the strong overlap between MD and FWF is biologically plausible, as increased extracellular space would lead to higher overall diffusivity.

Together, these relationships suggest that MD alterations in DLB reflect both cellular (neurite loss) and extracellular (increased free water) pathological changes. The substantial overlap between our MD and tNDI results implies that previous DTI studies using MD as a measure of microstructural integrity in DLB and other neurodegenerative disorders may have indeed been capturing changes in neurite density[18,22,23].

After delineating the spatial topography corresponding to gray matter microstructural injury in the DLB spectrum group, our next aim was to characterize the multivariate pathological pathways underlying the observed pattern of gray matter neurite abnormalities. The SEMs revealed an indirect chain of influences linking factors of age and APOE genotype to increased amyloid-β, which was, in turn, associated with greater tau burden, culminating in the neurite degeneration manifested by elevated MD, reduced tNDI, and ODI. Interestingly, this pathogenic sequence is well aligned with the "amyloid cascade hypothesis"[57], such that APOE and amyloid-β orchestrate downstream neurodegeneration in DLB through mechanistic pathways comparable to those implicated in AD[58]. Within this framework, APOE-related amyloid-β accumulation acts as the initiating trigger that sets off a cascade of downstream events, with tau implicated as the nexus connecting upstream amyloid-β accumulation to downstream neurite degeneration[59]. While the precise cellular mechanisms relating tau to NODDI parameters in DLB remain to be fully elucidated in the absence of post-mortem studies, corroborating data from tau transgenic mice models has demonstrated a significant loss of dendritic spines and synapses, likely mediated by tau-induced microtubule destabilization, dendritic retraction, and loss[60].

Our SEM analyses revealed a distinct pattern for FWF compared to other diffusion metrics, with amyloid showing direct effects on increased FWF ($\beta = 0.445$, $p = 0.027$, $R^2 = 0.392$) without the tau mediation that characterized MD, tNDI, and ODI. This direct relationship between amyloid and increased FWF aligns with emerging evidence that free-water imaging may be particularly sensitive to early amyloid-related changes. In support of this, recent work has demonstrated that increased FWF distinguishes plasma amyloid-positive from amyloid-negative individuals, even before demonstrable PET amyloid positivity[61]. Given that increased free water reflects neuroinflammation in the extracellular space[42], the direct relationship between amyloid and FWF may reflect early amyloid-induced neuroinflammatory responses[62]. Future studies incorporating α-synuclein biomarkers will be crucial to determine whether elevated FWF might represent a unique signature of α-synuclein-related pathology in DLB, distinct from AD-related neurodegeneration captured by other diffusion metrics[63].

Complementary to the SEM findings, our regional analyses revealed that temporal lobe tau burden predicted spatially specific patterns of neurite changes in the temporal lobe, with peak effects localized within the middle temporal gyrus. Previous studies have demonstrated the localized influence of medial temporal lobe tau on spatially specific neurodegeneration across the spectrum of cognitively unimpaired individuals[64] and those with MCI or AD[65]. Our findings extend this concept by demonstrating the existence of a similar phenomenon in the spectrum of DLB and showing that these effects may occur on a more granular cellular scale of neurite changes, beyond the macroscopic alterations in gray matter volume or cortical thickness. In contrast to the significant associations observed between tau burden and neurite changes, amyloid deposition did not exert independent influences on any of the DTI or NODDI parameters. This finding is in keeping with the lack of direct effects of amyloid on neurite microstructure in the aforementioned SEMs, suggesting that amyloid pathology may indirectly contribute to neurodegeneration through its influence on tau accumulation[66,67].

While our SEM analyses demonstrate relationships supporting aspects of the amyloid cascade hypothesis in DLB, it may only represent one of several pathogenic pathways in DLB. Interestingly, when the group comparison maps (Fig. 1) were juxtaposed against the topography of tau-related neurite injury (Fig. 3), it became evident that multiple regions exhibited neurite abnormalities in DLB compared to controls that were not specifically associated with tau pathology. This observation dovetails with the reported R2 values from our multivariate SEMs, which captured only a moderate proportion of the variability in neurite abnormalities (20–37%), indicating substantial contributions from pathogenic processes beyond the amyloid cascade, the most likely candidate being α-synuclein, either independently or through interactions with tau. Indeed, α-synuclein pathology has been shown to lead to selective decreases in synaptic proteins, progressive impairments in neuronal excitability and connectivity, and neuronal death[68]. Overexpression of α-synuclein in transgenic animal models has also been associated with pronounced cortical dendritic spine abnormalities, including reduced spine density and aberrant morphology[69]. Moreover, accumulating evidence suggests that the pathogenic effects of α-synuclein may be exacerbated by its interactions with tau pathology through a process of co-seeding, likely facilitated by the spatial co-localization of α-synuclein and tau within Lewy bodies[70]. Specifically, in vitro studies have demonstrated that α-synuclein fibrils can template the aggregation of tau into insoluble filaments, while tau aggregates can reciprocally induce the fibrillization of α-synuclein[71], leading to a toxic pathological loop with downstream effects on neuronal architecture[72]. Future studies incorporating measures of α-synuclein pathology, such as CSF or PET biomarkers, may help elucidate the relative contributions of α-synuclein and tau to neurite degeneration in DLB and their potential interactions.

The relationship between WMH and microstructural measures was generally limited and selective in our study. While WMH showed no associations with MD, tNDI, or ODI in either our SEM analyses or regional investigations, increased hippocampal FWF was specifically associated with greater WMH burden. This lack of widespread associations between WMH and most microstructural measures may reflect the complex and indirect mechanisms by which cerebrovascular disease influences gray matter structure[73] Furthermore, although our SEMs were predicated on the assumption that WMHs exert an influence on gray matter microstructure, the opposite scenario is that WMHs are a secondary phenomenon arising from axonal degeneration due to neuronal injury (i.e., Wallerian degeneration), which remains a viable consideration[74].

The relationships between microstructural measures and clinical features in DLB revealed complex patterns. While MD, tNDI, and ODI showed no significant associations with visual hallucinations, cognitive fluctuations, or parkinsonism, we observed a weak but significant positive correlation between FWF and UPDRS-III scores. This selective association between FWF and motor severity suggests that increased extracellular fluid may reflect specific aspects of neurodegeneration related to parkinsonian symptoms, potentially through increased oxidative stress[75], neuroinflammatory mechanisms[76] or tissue degradation in motor circuits. Notably, unlike MD and tNDI which showed strong associations with tau pathology, FWF did not correlate with either tau or amyloid burden, pointing to a distinct aspect of neurodegeneration more specific to Lewy body pathology. This finding aligns with and extends previous research in PD that demonstrated correlations between elevated free water levels and UPDRS-III scores[75], raising the hypothesis that extracellular fluid changes may be a common mechanism underlying motor symptoms across the Lewy body disease spectrum, though the precise biological mechanisms linking increased extracellular fluid to motor symptoms require further investigation.

Intriguingly, the DLB spectrum group with a clinical history of RBD exhibited increased ODI, which initially seems contradictory to the expected patterns of gray matter neurodegeneration. However, accumulating evidence from multimodal neuroimaging studies points to a more nuanced picture regarding RBD and imaging changes[63]. Paradoxically, RBD has been associated with decreased WMH[77] and *increased* gray matter volumes[78]. Additionally, autopsy studies have shown that DLB cases with RBD tend to have minimal AD copathologies[79] or fewer NFTs and amyloid plaques, possibly leading to better preservation of dendritic complexity[80]. Consistent with these findings, our post-hoc supplemental analyses indicated significantly lower tau burden in the RBD-positive group (Supplemental Table 1). Given the cross-sectional design and limited data, especially in the RBD-

negative group, these findings should be interpreted with caution and viewed as exploratory in nature.

Our study has several limitations that merit avenues for future research. Although we did not have autopsy confirmation in this study, the uncertainty of antemortem diagnosis is mitigated by the high autopsy confirmation rates of clinical diagnosis at our center (89%)[77]. The predominant male composition of our cohort is another limitation that may not fully represent the disease course in female patients with DLB. Nevertheless, we have previously shown that sex differences in gray matter network properties observed in healthy elderly individuals were diminished in DLB patients[81]. This suggests a disease-driven convergence of neurodegenerative patterns in women and men with DLB. However, we cannot exclude the possibility that important sex-specific patterns in the early stages of the disease or in comparison to healthy controls may have been missed. Moreover, the sex imbalance is unlikely to have led to false positives since previous research has indicated that women with DLB may have a more aggressive disease course, severity of cognitive impairment, and higher rates of AD biomarker positivity[12]. Further studies with larger, more balanced cohorts are needed to characterize sex-specific profiles of disease progression and treatment response across the DLB spectrum. The interpretation of our findings regarding increased ODI in the RBD-positive group warrants caution due to several limitations too. Firstly, the small sample size, particularly in the RBD-negative group, limits the robustness of our ODI comparisons between subgroups. Additionally, while our study included both prodromal ($n = 14$) and probable DLB ($n = 43$) patients to examine microstructural changes across the DLB severity spectrum, the relatively small sample size of the prodromal group limited our ability to conduct stratified analyses to evaluate potential stage-dependent differences in GM microstructure. Future studies with larger, more balanced cohorts are needed to specifically examine differences in diffusion metrics between prodromal and probable DLB, which could provide valuable insights into the progression of microstructural changes throughout the disease course. Such studies should consider longitudinal designs to track changes in diffusion metrics as individuals progress from prodromal to probable DLB stages. Secondly, not all participants classified as having RBD had polysomnography confirmation. Although the structure of our SEMs (placement of variables) was designed with biological plausibility[58], longitudinal studies are ultimately needed to establish change rates of NODDI parameters across the DLB spectrum and how they may relate to the progressive accumulation of tau[11] and amyloid-β over time[82]. While our cross-sectional analyses suggest that NODDI can detect microstructural abnormalities after controlling for gray matter volumes, we acknowledge that our current study design does not directly prove their superior sensitivity to subtle changes. Our findings should, therefore, be interpreted as preliminary evidence warranting further investigation. Future longitudinal studies specifically designed to examine the temporal relationship between NODDI metrics and cortical thinning in DLB would provide more definitive evidence to determine whether NODDI metrics could detect microstructural changes preceding macroscopic atrophy. Such studies comparing tNDI and MD changes with macrostructural measures across different stages of DLB are needed to definitively establish their relative sensitivity to disease progression. These studies could stratify patients by disease severity or use repeated measures over time to capture the earliest detectable changes, ultimately establishing the potential of these microstructural measures as early biomarkers of neurodegeneration in DLB. Future studies following a cohort of MCI-LBs would be highly anticipated to delineate the baseline cortical signatures of MD, tNDI, and ODI that best predict the clinical transition to probable DLB. The absence of correlations between NODDI metrics and clinical features in our cross-sectional analysis does not necessarily negate the potential value of NODDI too. Future planned longitudinal studies may reveal that changes in NODDI metrics over time are predictive of future clinical decline, even if these metrics do not correlate strongly with current symptoms in a cross-sectional design. While current interpretations suggest gray matter NDI and ODI metrics may serve as proxies of synaptic density[39] and dendritic arborization[36,83], further studies are still needed to establish the histological basis of NODDI in human gray matter[32]. Our methodology of using an AD-characteristic meta-ROI to quantify tau burden facilitates comparison with existing AD literature and other tau PET imaging studies in DLB, focusing on clinically relevant tau deposition in DLB[51,84]. However, this approach is not without limitations. Firstly, it could potentially underestimate tau pathology in regions more specific to DLB. Secondly, it may not fully capture the topography of microstructural injury that is more intrinsic to DLB-specific tau propagation, particularly in areas influenced by alpha-synuclein spread independent of amyloid[85]. At present, there is a lack of consensus on a DLB-specific meta-ROI for tau deposition, and the development or validation of such a measure extends beyond the scope of our current study. Furthermore, the inability to account for regional α-synuclein pathology is a limitation of our study, precluding a comprehensive analysis of the inter-relationships between α-synuclein, AD copathologies, microstructural injury, and downstream clinical manifestations. Future studies should incorporate emerging α-synuclein biomarkers, such as PET imaging[86] or detection of CSF α-synuclein by RT-QuIC[87], alongside AD biomarkers and NODDI within a multimodal paradigm. This approach would allow for a more comprehensive characterization of our SEMs and help understand how distinct pathological processes may influence the clinical symptoms of DLB, thereby disentangling additive versus synergistic pathways leading to neurite alterations and clinical decline.

Our NODDI study revealed widespread regional gray matter microstructural abnormalities in DLB, with tau emerging as a critical nexus in the amyloid cascade. Our findings, combined with recent evidence showing mild clinical benefits of anti-amyloid therapies in AD, suggest that targeting amyloid-β alone may be insufficient for improving clinical outcomes in DLB. The complex interactions between amyloid-β, tau, and alpha-synuclein pathologies on microstructural changes in the DLB spectrum support that a multi-target therapeutic approach may yield the greatest therapeutic potential.

Materials

Participants

We included consecutive patients with clinically probable DLB[2] with dementia that ranged from mild to moderate severity ($n = 43$) and those with prodromal DLB ($n = 14$) defined as MCI with Lewy bodies[88] to comprise a group of people on the DLB spectrum ($n = 57$) who were enrolled at the Mayo Clinic Alzheimer's Disease Research Center (ADRC) between January 2018 and February 2023. Of the 57 participants in the DLB spectrum group, 50 underwent dopamine transporter (DAT) imaging either at the time of the DTI visit or at an earlier visit. Among these, 43 had abnormal DAT scans, and seven had normal DAT scans. Clinical diagnosis was established by a consensus committee including behavioral neurologists, neuropsychologists, and study coordinators. Clinical evaluations included a neurologic examination and standardized instruments for the assessment of cognitive performance and activities of daily living. Clinical disease severity was measured with the clinical dementia rating, sum-of-box scores (CDR-SB), and global cognitive performance was evaluated with the Mini-Mental State Examination (MMSE)[89]. We also assessed clinical features characteristic of DLB: (1) Unified Parkinson Disease Rating Scale, part III (UPDRS-III) for parkinsonism; (2) visual hallucinations characterized by being fully formed, not restricted to a single episode and not related to another medical issue; (3) cognitive fluctuations defined as a score of 3 or 4 on the Mayo Fluctuations Questionnaire[90]; and (4) probable REM sleep behavior disorder (RBD) based on the minimal diagnostic criteria for RBD diagnosis according to the International Classification of Sleep Disorders-II[91,92]. In addition, we included a CU group from the population-based Mayo Clinic Study of Aging, an epidemiologic study

of aging in Olmsted County, MN[93], matched 1:1 on age and sex with the DLB group using an automated greedy match algorithm. Study participants met specific inclusion criteria, including having undergone 3T MRI, multi-shell diffusion-weighted imaging, amyloid, and tau PET scans. Exclusion criteria for the DLB spectrum group were a history of traumatic brain injury, hydrocephalus or intracranial mass, a history of chemotherapy, head radiation therapy, or substance abuse, and having neurologic or psychiatric disorders other than prodromal or probable DLB. CU participants with any neurologic or psychiatric disease were also excluded. The Mayo Clinic Institutional Review Board approved the study. Informed consent for participation was obtained from participants or their legally authorized representative, according to the Declaration of Helsinki.

MRI and PET acquisitions

All participants received the same brain MRI protocol on one of three identical Siemens Prisma 3T scanners running VE11E software and equipped with a 64-channel receiver head coil. The protocol included T1, T2, and diffusion-weighted sequences. The T1-weighted magnetization-prepared rapid gradient echo (MPRAGE) scan had isotropic 0.8 mm resolution, 2x phase acceleration, 2300 ms repetition time, 3.1 ms echo time, and flip angle 9o. The T2-weighted acquisition used a 3D SPACE sequence with isotropic 0.8 mm resolution, 2x phase acceleration, 3200 ms repetition time, 564 ms echo time, and flip angle 120°. The diffusion acquisition used 3x simultaneous multi-slice acceleration with adaptive coil combination and 2.0 mm isotropic voxels. The diffusion data consisted of 127 volumes, including 13 non-diffusion-weighted images and 114 diffusion-encoding gradient directions. The diffusion-weighted images were evenly spread using an electrostatic repulsion model35 over entire spherical shells at b = 0, 500, 1000, and 2000 s/mm^2 and were interspersed in time to minimize gradient heating. The echo time and repetition time were 71 and 3400 ms, respectively. PET imaging was performed on Siemens and General Electric PET/CT scanners. The 11C-PiB scans were 20-minute static frames captured from 40 to 60 min post-injection (average 596 MBq; range 292–729 MBq). For Flortaucipir PET scans, an intravenous bolus injection of an average of 370 MBq (range 333–407 MBq) was administered, followed by an 80-min uptake period and a 20-min static scan. Detailed information on PET data preprocessing can be found in our previous studies[11,52,94].

Preprocessing

We used an in-house pipeline to preprocess the diffusion datasets, which were visually inspected for quality by trained analysts. An intracranial mask was created for the diffusion MRI scan[95], and the noise was estimated and removed using random matrix theory[96]. Head motion and eddy current distortion were corrected using FSL's eddy_cuda[97], followed by correction of Gibbs ringing[98] and Rician bias correction[99]. We addressed susceptibility-induced geometric distortions through structural MRI-guided correction6, where a T1-like contrast image was synthesized from the diffusion data and warped to the undistorted T1-weighted image to minimize geometric mismatch, allowing for correction of spatial misregistration between diffusion and anatomical images. Diffusion tensors were fitted using a non-linear least-squares fitting algorithm implemented in DIPY (https://dipy.org/index.html) to generate MD images from the extracted b = 1000 data. The NODDI model was fitted using the accelerated microstructure imaging via convex optimization (AMICO, https://github.com/daducci/AMICO) implementation in Python[100], producing voxelwise maps of ODI, NDI, and FWF. Consistent with our previous study[20], tissue-weighted NDI (tNDI) maps were generated by adjusting the original NDI maps with a scaling factor (1-FWF), which accounts for the presence of free water, cerebrospinal fluid, and other extracellular spaces. To generate regional measures of MD, tNDI, ODI, and FWF for each gray matter region, we first registered the Mayo Clinic Adult Lifespan Template (MCALT) atlas[101] to participant T1 MRI native space using advanced normalization tools—symmetric normalization (https://stnava.github.io/ANTs/). Subsequently, we applied the corresponding warps to their diffusion MRI native space[102]. Regions in the cerebellum were excluded a priori, resulting in a final set of 43 regions of interest (ROIs) (Supplemental Table 1). Next, bilateral median values of MD, tNDI, and ODI, FWF were computed and weighted by the size of each ROI.

PET images were analyzed using our fully automated in-house image processing pipeline[103]. Each tau PET image was rigidly registered to its corresponding MPRAGE using SPM12[104], and regional PET values were extracted from automatically labeled ROIs propagated from the MCALT[101]. For each participant scan, we calculated a composite cortical amyloid-β standardized uptake value ratio (SUVr) by taking the median uptake in six ROIs: prefrontal, orbitofrontal, parietal, temporal, anterior cingulate, and posterior cingulate/precuneus, and normalizing by the median amyloid-β PET uptake in the cerebellar crus gray matter. Similarly, we computed a composite Flortaucipir SUVr by taking the median tau PET uptake in six ROIs: entorhinal, amygdala, parahippocampal, fusiform, inferior temporal, and middle temporal, and normalizing by the median tau PET uptake in the cerebellar crus gray matter for each participant. These composite SUVr values provided cortical summary measures of amyloid-β and tau uptake (Fig. 5), which were subsequently used as predictors in our SEMs to investigate multivariate associations with gray matter MD, tNDI, and ODI.

Tissue probabilities for each MPRAGE were estimated using the unified segmentation algorithm in SPM12 with Mayo Clinic Adult Lifespan Template (MCALT) tissue priors and settings. The MCALT atlases were propagated into each individual's native space to estimate regional gray matter volumes, expressed as a percentage of total intracranial volume (TIV). The WMH volume was quantified from 3D FLAIR images using a fully automated updated version of a method as previously described[105].

Statistical analyses

Demographic and clinical characteristics were reported using mean values and standard deviations for continuous variables and counts and percentages for categorical variables. WMH was normalized by total intracranial volume and reported as a percentage. A log transformation was done to improve the distribution of data and model fitting. Cortical Flortaucipir and PiB SUVr values were also analyzed with a log-transformation. We used conditional logistic regression models to compare regional differences of MD, tNDI, ODI, and FWF between the DLB spectrum and CU controls, accounting for the 1:1 matching between subjects. To assess whether group differences in MD, tNDI, ODI, and FWF were independent of gray matter atrophy, we repeated the conditional logistic regressions and controlled for regionally specific gray matter volumes (expressed as a percentage of TIV). *P* values were adjusted with the false discovery rate (FDR) method for multiple testing across the ROIs. An adjusted FDR q value ≤0.05 (two-tailed) was considered significant. These results were used to derive composite ROIs representing the spatial distribution of microstructural abnormalities in gray matter within the DLB spectrum group. Subsequently, Dice coefficient indices were computed between binarized maps representing the FDR-corrected group differences. The formula for the Dice coefficient is as follows: $\text{Dice} = 2 \times (A \cap B)/(A + B)$, where A and B are the two binarized maps. To delineate the multivariate relationships among age, APOE genotype, amyloid-β, tau, WMH, and composite ROIs, path analyses (SEMs with only manifest variables) were employed using Mplus version 8.10. PiB and Flortaucipir SUVR and WMH (as %TIV) were log-transformed, age was in decades, and MD was divided by 100 in the SEMs. Age and APOE genotype were included in the model as predictors of both AD biomarkers and gray matter microstructural injury in the DLB spectrum. Backward elimination pruning was used to derive parsimonious models, which considered direct effects (immediate relationships between variables), indirect effects mediated through one or more other variables, and total effects, representing the sum of direct and indirect pathways. To obtain a measure of effect sizes, we also reported R-squares for each of the outcome variables in the SEMs. Given that our SEMs might only reveal AD associations in regions with group-

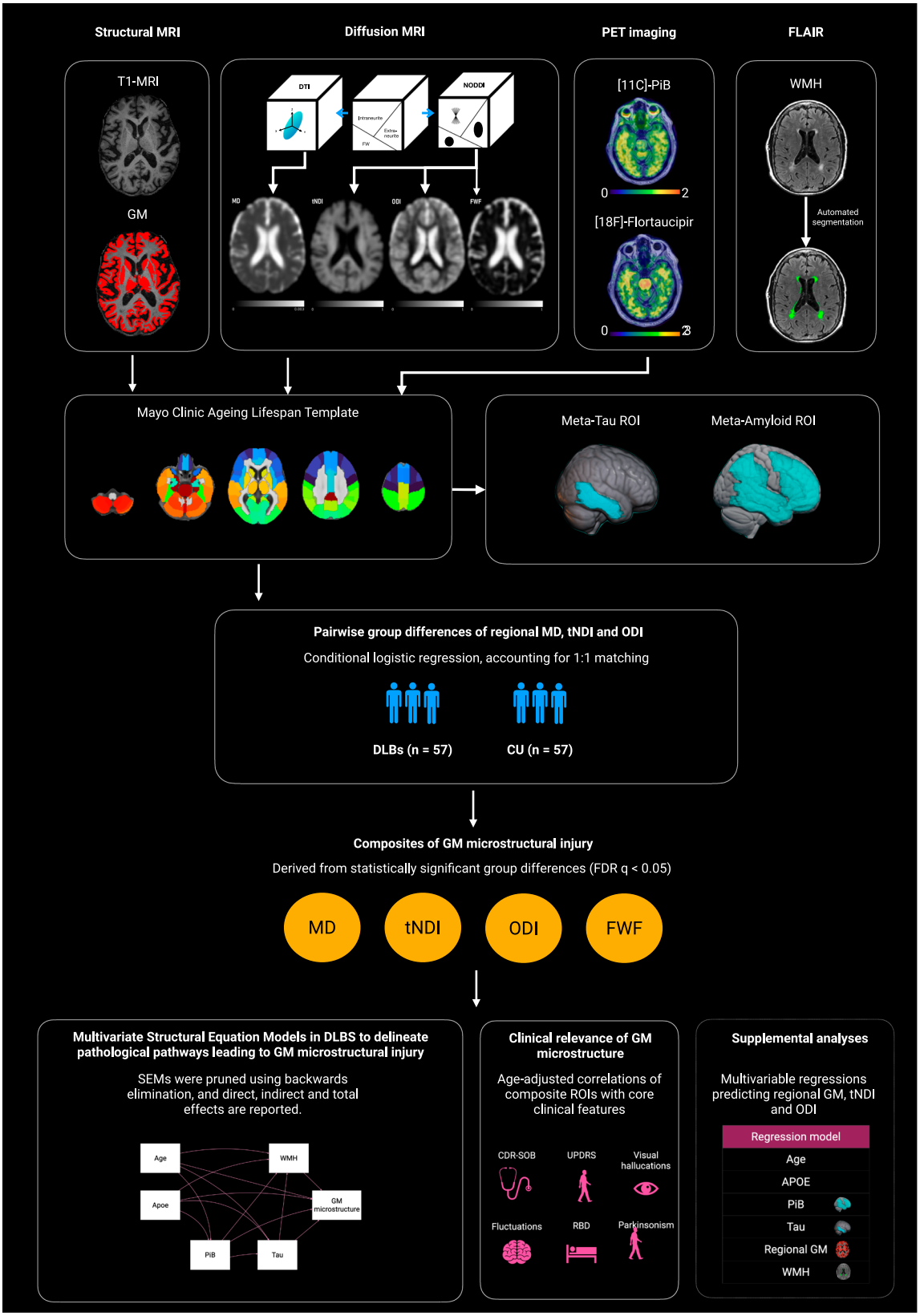

level differences between the DLB spectrum and CU controls, we pursued multivariable regression analyses to assess associations between both AD biomarkers and regional MD, tNDI, ODI, and FWF adjusted for age, APOE, gray matter volumes, and WMH. To explore whether the spatial patterns of gray matter microstructural injury relate to the severity of core clinical features that are characteristic of DLB, we ran age-adjusted partial Pearson correlations between composite ROIs of MD, tNDI, ODI, and FWF with CDR-SB, UPDRS-III, and duration of years of core clinical features: visual hallucinations, cognitive fluctuations, parkinsonism, and REM sleep behavior

Fig. 5 | Graphical overview of the study design and key analyses. The study design involved fitting diffusion-weighted imaging datasets with DTI and NODDI models to obtain whole-brain maps of MD, tNDI, ODI, and FWF. Participants underwent PET imaging of PiB and Flortaucipir to quantify amyloid-β and tau deposition, respectively. Regional gray matter volumes were derived from structural MRI using SPM12. WMHs were calculated from FLAIR using an automated segmentation technique. The voxelwise MD, tNDI, ODI, and FWF parameter maps were parcellated using the MCALT atlas to derive bilateral median values reflecting regional GM microstructural integrity. We employed conditional logistic models to compare regional MD, tNDI, ODI, and FWF between the DLB spectrum and CU groups. Subsequently, statistically significant ROIs from the group-wise comparisons were used as composite outcome measures in SEMs to determine their multivariate associations with age, WMH, APOE genotype, amyloid-β, and tau. In exploratory analyses, partial Pearson's correlations were used to determine the degree to which composites of MD, tNDI, ODI, and FWF are related to disease severity and core features in the DLB spectrum. Supplemental regression analyses were used to explore the topographical associations of tau and amyloid PET meta-ROIs with regionally specific MD, tNDI, ODI, and FWF, irrespective of group differences. These models were adjusted for age, APOE genotype, gray matter volumes (expressed as the % of TIV), and WMH (expressed as the % of TIV). AD Alzheimer's disease, APOE apolipoprotein E, CDR-SB clinical dementia rating-sum of boxes, CU cognitively unimpaired, DLB dementia with Lewy bodies, DTI diffusion tensor imaging, FDR false discovery rate, *FLAIR* fluid-attenuated inversion recovery, *FWF* free water fraction, GM gray matter, *TIV* total intracranial volume, MCALT Mayo clinic adult lifespan template, MD mean diffusivity, NODDI neurite orientation dispersion and density imaging, ODI orientation dispersion index, PET positron emission tomography, Amyloid-β Pittsburgh compound B, RBD REM sleep behavior disorder, ROIs regions of interest, SEM structural equation modeling, tNDI tissue-weighted neurite density index, UPDRS unified Parkinson's disease rating scale, WMH white matter hyperintensity.

disorder. Additionally, we compared these composite ROIs between DLB subgroups categorized by the presence or absence of core clinical features with ANCOVA models adjusting for age.

Data availability

Anonymized data will be shared in accordance with the Mayo ADRC data sharing protocol upon request from a qualified investigator to the corresponding author. An acceptable Data Use Agreement is required, which specifies the terms and conditions for secure data storage, protection, and compliance with data protection regulations and ethical guidelines.

Code availability

The *R* analysis scripts used for the statistical analyses in this study are provided in the Supplementary Material. Additional code is available from the corresponding author upon request.

Received: 24 June 2024; Accepted: 18 March 2025;
Published online: 12 May 2025

References

1. Vann Jones, S. A. & O'Brien, J. T. The prevalence and incidence of dementia with Lewy bodies: a systematic review of population and clinical studies. *Psychol. Med.* **44**, 673–683 (2013).
2. McKeith, I. G. et al. Diagnosis and management of dementia with Lewy bodies. *Neurology* **89**, 88–100 (2017).
3. McKeith, I. G. et al. Diagnosis and management of dementia with Lewy bodies: third report of the DLB consortium. *Neurology* **65**, 1863–1872 (2005).
4. Ferman, T. J. et al. The limbic and neocortical contribution of α-Synuclein, tau, and amyloid β to disease duration in dementia with Lewy bodies. *Alzheimers Dement.* **14**, 330–339 (2018).
5. Walker, L. et al. Neuropathologically mixed Alzheimer's and Lewy body disease: burden of pathological protein aggregates differs between clinical phenotypes. *Acta Neuropathol.* **129**, 729–748 (2015).
6. Irwin, D. J. et al. Neuropathological and genetic correlates of survival and dementia onset in synucleinopathies: a retrospective analysis. *Lancet Neurol.* **16**, 55–65 (2017).
7. Dickson, D. W. et al. APOE ε4 is associated with severity of Lewy body pathology independent of Alzheimer pathology. *Neurology* **91**, e1182–e1195 (2018).
8. Jin, Y. et al. APOE4 exacerbates α-synuclein seeding activity and contributes to neurotoxicity in Alzheimer's disease with Lewy body pathology. *Acta Neuropathol.* **143**, 641–662 (2022).
9. Kantarci, K. et al. Focal atrophy on MRI and neuropathologic classification of dementia with Lewy bodies. *Neurology* **79**, 553–560 (2012).
10. Nedelska, Z. et al. Pattern of brain atrophy rates in autopsy-confirmed dementia with Lewy bodies. *Neurobiol. Aging* **36**, 452–461 (2015).
11. Chen, Q. et al. Longitudinal Tau positron emission tomography in dementia with Lewy bodies. *Mov. Disord.* **37**, 1256–1264 (2022).
12. Ferreira, D. et al. Cross-sectional associations of β-Amyloid, tau, and cerebrovascular biomarkers with neurodegeneration in probable dementia with lewy bodies. *Neurology* **100**, e846–e859 (2022).
13. Mak, E. et al. Beta amyloid deposition maps onto hippocampal and subiculum atrophy in dementia with Lewy bodies. *Neurobiol. Aging* **73**, 74–81 (2019).
14. Sarro, L. et al. Amyloid-β deposition and regional grey matter atrophy rates in dementia with Lewy bodies. *Brain J. Neurol.* **139**, 2740–2750 (2016).
15. Shimada, H. et al. β-amyloid in lewy body disease is related to Alzheimer's disease-like atrophy. *Mov. Disord.* **28**, 169–175 (2012).
16. Merino-Serrais, P. et al. The influence of phospho-tau on dendritic spines of cortical pyramidal neurons in patients with Alzheimer's disease. *Brain* **136**, 1913–1928 (2013).
17. Le Bihan, D. et al. Diffusion tensor imaging: concepts and applications. *J. Magn. Reson. Imaging* **13**, 534–546 (2001).
18. Firbank, M. J. et al. Longitudinal diffusion tensor imaging in dementia with Lewy bodies and Alzheimer's disease. *Parkinsonism Relat. Disord.* **24**, 76–80 (2016).
19. Kantarci, K. et al. Dementia with Lewy bodies and Alzheimer disease: neurodegenerative patterns characterized by DTI. *Neurology* **74**, 1814–1821 (2010).
20. Mak, E. et al. White matter neurite alterations in dementia with Lewy body bodies: influence of amyloid-β and tau. *Nat. Park. Dis*. (2024).
21. Mak, E., Su, L., Williams, G. B. & O'Brien, J. T. Neuroimaging characteristics of dementia with Lewy bodies. *Alzheimers Res. Ther.* **6**, 18 (2014).
22. Nedelska, Z. et al. White matter integrity in dementia with Lewy bodies: a voxel-based analysis of diffusion tensor imaging. *Neurobiol. Aging* **36**, 2010–2017 (2015).
23. Watson, R. et al. Characterizing dementia with Lewy bodies by means of diffusion tensor imaging. *Neurology* **79**, 906–914 (2012).
24. Mak, E. et al. Multi-modal MRI investigation of volumetric and microstructural changes in the hippocampus and its subfields in mild cognitive impairment, Alzheimer's disease, and dementia with Lewy bodies. *Int. Psychogeriatr.* **29**, 545–555 (2017).
25. Weston, P. S. J., Simpson, I. J. A., Ryan, N. S., Ourselin, S. & Fox, N. C. Diffusion imaging changes in grey matter in Alzheimer's disease: a potential marker of early neurodegeneration. *Alzheimers Res. Ther.* **7**, 47 (2015).
26. Weston, P. S. J. et al. Measuring cortical mean diffusivity to assess early microstructural cortical change in presymptomatic familial Alzheimer's disease. *Alzheimers Res. Ther.* **12**, 112 (2020).

27. Kantarci, K. et al. DWI predicts future progression to Alzheimer disease in amnestic mild cognitive impairment. *Neurology* **64**, 902–904 (2005).
28. Henf, J., Grothe, M. J., Brueggen, K., Teipel, S. & Dyrba, M. Mean diffusivity in cortical gray matter in Alzheimer's disease: the importance of partial volume correction. *Neuroimage Clin.* **17**, 579–586 (2017).
29. Jones, D. K., Knösche, T. R. & Turner, R. White matter integrity, fiber count, and other fallacies: the do's and don'ts of diffusion MRI. *NeuroImage* **73**, 239–254 (2013).
30. Zhang, H., Schneider, T., Wheeler-Kingshott, C. A. & Alexander, D. C. NODDI: practical in vivo neurite orientation dispersion and density imaging of the human brain. *Neuroimage* **61**, 1000–1016 (2012).
31. Parker, C. S. et al. Not all voxels are created equal: reducing estimation bias in regional NODDI metrics using tissue-weighted means. *Neuroimage* **245**, 118749 (2021).
32. Grussu, F. et al. Neurite dispersion: a new marker of multiple sclerosis spinal cord pathology?. *Ann. Clin. Transl. Neurol.* **4**, 663–679 (2017).
33. Raghavan, S. et al. Diffusion models reveal white matter microstructural changes with ageing, pathology and cognition. *Brain Commun.* **3**, fcab106 (2021).
34. Adluru, N. et al. White matter microstructure in late middle-age: effects of apolipoprotein E4 and parental family history of Alzheimer's disease. *Neuroimage Clin.* **4**, 730–742 (2014).
35. Motovylyak, A. et al. Age-related differences in white matter microstructure measured by advanced diffusion MRI in healthy older adults at risk for Alzheimer's disease. *Aging Brain* **2**, 100030 (2022).
36. Mak, E. et al. APOE ε4 exacerbates age-dependent deficits in cortical microstructure. *Brain Commun.* **6**, fcad351 (2024).
37. Parker, T. D. et al. Cortical microstructure in young onset Alzheimer's disease using neurite orientation dispersion and density imaging. *Hum. Brain Mapp.* **39**, 3005–3017 (2018).
38. Corriveau-Lecavalier, N. et al. Neurite-based white matter alterations in MAPT mutation carriers: a multi-shell diffusion MRI study in the ALLFTD consortium. *Neurobiol. Aging* **134**, 135–145 (2024).
39. Mak, E. et al. In vivo coupling of dendritic complexity with presynaptic density in primary tauopathies. *Neurobiol. Aging* **101**, 187–198 (2021).
40. Maillard, P. et al. MRI free water as a biomarker for cognitive performance: validation in the MarkVCID consortium. *Alzheimers Dement. Diagn. Assess. Dis. Monit.* **14**, e12362 (2022).
41. Ofori, E. et al. Free-water imaging of the hippocampus is a sensitive marker of Alzheimer's disease. *Neuroimage Clin.* **24**, 101985 (2019).
42. Pasternak, O., Sochen, N., Gur, Y., Intrator, N. & Assaf, Y. Free water elimination and mapping from diffusion MRI. *Magn. Reson. Med.* **62**, 717–730 (2009).
43. Kamiya, K., Hori, M. & Aoki, S. NODDI in clinical research. *J. Neurosci. Methods* **346**, 108908 (2020).
44. Vogt, N. M. et al. Cortical microstructural alterations in mild cognitive impairment and Alzheimer's disease dementia. *Cereb. Cortex* **30**, 2948–2960 (2020).
45. Colom-Cadena, M. et al. Synaptic phosphorylated α-synuclein in dementia with Lewy bodies. *Brain J. Neurol.* **140**, 3204–3214 (2017).
46. Revuelta, G. J., Rosso, A. & Lippa, C. F. Neuritic pathology as a correlate of synaptic loss in dementia with Lewy bodies. *Am. J. Alzheimers Dis. Other Demen.* **23**, 97–102 (2008).
47. DeTure, M. A. & Dickson, D. W. The neuropathological diagnosis of Alzheimer's disease. *Mol. Neurodegener.* **14**, 32 (2019).
48. Kantarci, K. et al. FDG PET metabolic signatures distinguishing prodromal DLB and prodromal AD. *Neuroimage Clin.* **31**, 102754 (2021).
49. Delli Pizzi, S. et al. Structural connectivity is differently altered in dementia with Lewy body and Alzheimer's disease. *Front. Aging Neurosci.* **7**, 208 (2015).
50. Nedelska, Z. et al. Regional cortical perfusion on arterial spin labeling MRI in dementia with Lewy bodies: associations with clinical severity, glucose metabolism and tau PET. *Neuroimage Clin.* **19**, 939–947 (2018).
51. Gomperts, S. N. et al. Tau positron emission tomographic imaging in the Lewy body diseases. *JAMA Neurol.* **73**, 1334 (2016).
52. Kantarci, K. et al. AV-1451 tau and β-Amyloid positron emission tomography imaging in dementia with Lewy bodies. *Ann. Neurol.* **81**, 58–67 (2016).
53. Deligianni, F., Carmichael, D. W., Zhang, G. H., Clark, C. A. & Clayden, J. D. NODDI and tensor-based microstructural indices as predictors of functional connectivity. *PLoS ONE* **11**, e0153404 (2016).
54. Nazeri, A. et al. Functional consequences of neurite orientation dispersion and density in humans across the adult lifespan. *J. Neurosci.* **35**, 1753–1762 (2015).
55. Fukutomi, H. et al. Neurite imaging reveals microstructural variations in human cerebral cortical gray matter. *Neuroimage* **182**, 488–499 (2018).
56. Zaja-Milatovic, S. et al. Selective dendritic degeneration of medium spiny neurons in dementia with Lewy bodies. *Neurology* **66**, 1591–1593 (2006).
57. Hardy, J. A. & Higgins, G. A. Alzheimer's disease: the amyloid cascade hypothesis. *Science* **256**, 184–185 (1992).
58. Jack, C. R. et al. Update on hypothetical model of Alzheimer's disease biomarkers. *Lancet Neurol.* **12**, 207–216 (2013).
59. Shi, Y. et al. ApoE4 markedly exacerbates tau-mediated neurodegeneration in a mouse model of tauopathy. *Nature* **549**, 523–527 (2017).
60. Stamer, K., Vogel, R., Thies, E., Mandelkow, E. & Mandelkow, E.-M. Tau blocks traffic of organelles, neurofilaments, and APP vesicles in neurons and enhances oxidative stress. *J. Cell Biol.* **156**, 1051–1063 (2002).
61. DeSimone, J. C. et al. Diffusion MRI relates to plasma Aβ42/40 in PET negative participants without dementia. *Alzheimers Dement.* **20**, 2830–2842 (2024).
62. Craft, J. M., Watterson, D. M. & Van Eldik, L. J. Human amyloid beta-induced neuroinflammation is an early event in neurodegeneration. *Glia* **53**, 484–490 (2006).
63. Boeve, B. F. & Kantarci, K. Multimodal imaging in RBD - present and future. *Nat. Rev. Neurol.* **14**, 574–576 (2018).
64. Maass, A. et al. Entorhinal tau pathology, episodic memory decline, and neurodegeneration in aging. *J. Neurosci.* **38**, 530–543 (2018).
65. Mak, E. et al. In vivo coupling of tau pathology and cortical thinning in Alzheimer's disease. *Alzheimers Dement. Diagn. Assess. Dis. Monit.* **10**, 678–687 (2018).
66. Kantarci, K. et al. White matter integrity on DTI and the pathologic staging of Alzheimer's disease. *Neurobiol. Aging* **56**, 172–179 (2017).
67. Kantarci, K. et al. White matter integrity determined with diffusion tensor imaging in older adults without dementia. *JAMA Neurol.* **71**, 1547 (2014).
68. Volpicelli-Daley, L. A. et al. Exogenous α-synuclein fibrils induce Lewy body pathology leading to synaptic dysfunction and neuron death. *Neuron* **72**, 57–71 (2011).
69. Blumenstock, S. et al. Seeding and transgenic overexpression of alpha-synuclein triggers dendritic spine pathology in the neocortex. *EMBO Mol. Med.* **9**, 716–731 (2017).
70. Ishizawa, T., Mattila, P., Davies, P., Wang, D. & Dickson, D. W. Colocalization of tau and alpha-synuclein epitopes in lewy bodies. *J. Neuropathol. Exp. Neurol.* **62**, 389–397 (2003).
71. Giasson, B. I. et al. Initiation and synergistic fibrillization of tau and alpha-synuclein. *Science* **300**, 636–640 (2003).

72. Moussaud, S. et al. Alpha-synuclein and tau: teammates in neurodegeneration? *Mol. Neurodegener*. **9**, 43 (2014).
73. Pantoni, L. Cerebral small vessel disease: from pathogenesis and clinical characteristics to therapeutic challenges. *Lancet Neurol.* **9**, 689–701 (2010).
74. Erten-Lyons, D. et al. Neuropathologic basis of white matter hyperintensity accumulation with advanced age. *Neurology* **81**, 977–983 (2013).
75. Ofori, E. et al. Free-water improves detection of changes in the substantia nigra in parkinsonism: a multi-site study. *Mov. Disord.* **32**, 1457–1464 (2017).
76. Surendranathan, A. et al. Early microglial activation and peripheral inflammation in dementia with Lewy bodies. *Brain J. Neurol.* **141**, 3415–3427 (2018).
77. Sarro, L. et al. An investigation of cerebrovascular lesions in dementia with Lewy bodies compared to Alzheimer's disease. *Alzheimers Dement.* **13**, 257–266 (2016).
78. Scherfler, C. et al. White and gray matter abnormalities in idiopathic rapid eye movement sleep behavior disorder: a diffusion-tensor imaging and voxel-based morphometry study. *Ann. Neurol.* **69**, 400–407 (2011).
79. Ferman, T. J. et al. Subtypes of dementia with Lewy bodies are associated with α-synuclein and tau distribution. *Neurology* **95**, e155–e165 (2020).
80. Murray, M. et al. RBD Is Associated with reduced Alzheimer's pathology in dementia with Lewy bodies (P05.050). *Neurology* **78**, P05.050–P05.050 (2012).
81. Habich, A. et al. Grey matter networks in women and men with dementia with Lewy bodies. *Npj Park. Dis.* **10**, 1–9 (2024).
82. Nedelska, Z. et al. Association of longitudinal β-amyloid accumulation determined by positron emission tomography with clinical and cognitive decline in adults with probable Lewy body dementia. *JAMA Netw. Open* **2**, e1916439 (2019).
83. Genç, E. et al. Diffusion markers of dendritic density and arborization in gray matter predict differences in intelligence. *Nat. Commun.* **9**, 1905 (2018).
84. Mak, E. et al. Imaging tau burden in dementia with Lewy bodies using [18F]-AV1451 positron emission tomography. *Neurobiol. Aging* **101**, 172–180 (2021).
85. Shim, K. H., Kang, M. J., Youn, Y. C., An, S. S. A. & Kim, S. Alpha-synuclein: a pathological factor with Aβ and tau and biomarker in Alzheimer's disease. *Alzheimers Res. Ther*. **14**, 201 (2022).
86. Kantarci, K. Toward imaging of alpha-synuclein with PET. *Cell* **186**, 3327–3329 (2023).
87. Iranzo, A. et al. Detection of α-synuclein in CSF by RT-QuIC in patients with isolated rapid-eye-movement sleep behaviour disorder: a longitudinal observational study. *Lancet Neurol.* **20**, 203–212 (2021).
88. McKeith, I. G. et al. Research criteria for the diagnosis of prodromal dementia with Lewy bodies. *Neurology* **94**, 743–755 (2020).
89. Folstein, M. F., Folstein, S. E. & McHugh, P. R. Mini-mental state. *J. Psychiatr. Res.* **12**, 189–198 (1975).
90. Ferman, T. J. et al. DLB fluctuations: specific features that reliably differentiate DLB from AD and normal aging. *Neurology* **62**, 181–187 (2004).
91. American Academy of Sleep Medicine. *Classification of Sleep Disorders, Second Edition (ICSD-2)*. (American Academy of Sleep Medicine, 2005).
92. Boeve, B. F. et al. Validation of the mayo sleep questionnaire to screen for REM sleep behavior disorder in a community-based sample. *J. Clin. Sleep. Med.* **09**, 475–480 (2013).
93. Roberts, R. O. et al. The Mayo clinic study of aging: design and sampling, participation, baseline measures and sample characteristics. *Neuroepidemiology* **30**, 58–69 (2008).
94. Diaz-Galvan, P. et al. β-amyloid load on PET along the continuum of dementia with Lewy bodies. *Neurology* **101**, e178–e188 (2023).
95. Reid, R. I. et al. Diffusion specific segmentation: skull stripping with diffusion MRI data alone. In *Computational Diffusion MRI MICCAI Workshop* (Springer International Publishing, 2018).
96. Veraart, J. et al. Denoising of diffusion MRI using random matrix theory. *Neuroimage* **142**, 394–406 (2016).
97. Andersson, J. L. R. & Sotiropoulos, S. N. An integrated approach to correction for off-resonance effects and subject movement in diffusion MR imaging. *Neuroimage* **125**, 1063–1078 (2016).
98. Kellner, E., Dhital, B., Kiselev, V. G. & Reisert, M. Gibbs-ringing artifact removal based on local subvoxel-shifts. *Magn. Reson. Med.* **76**, 1574–1581 (2015).
99. Koay, C. G., Ozarslan, E. & Basser, P. J. A signal-transformational framework for breaking the noise floor and its applications in MRI. *J. Magn. Reson.* **197**, 108–119 (2009).
100. Daducci, A. et al. Accelerated microstructure imaging via convex optimization (AMICO) from diffusion MRI data. *Neuroimage* **105**, 32–44 (2015).
101. Schwarz, C. G. et al. [P2–415]: the Mayo clinic adult lifespan template: better quantification across the lifespan. *Alzheimers Dement*. **13**, P792–P792 (2017).
102. Avants, B. B. et al. A reproducible evaluation of ANTs similarity metric performance in brain image registration. *Neuroimage* **54**, 2033–2044 (2011).
103. Jack, C. R. et al. The bivariate distribution of amyloid-β and tau: relationship with established neurocognitive clinical syndromes. *Brain J. Neurol.* **142**, 3230–3242 (2019).
104. Ashburner, J. Computational anatomy with the SPM software. *Magn. Reson. Imaging* **27**, 1163–1174 (2009).
105. Raz, L. et al. Thrombogenic microvesicles and white matter hyperintensities in postmenopausal women. *Neurology* **80**, 911–918 (2013).

Acknowledgements

This work was supported by the National Institute of Health [grants U01 NS100620 (PIs: Kantarci and Boeve), R01 AG40042 (PI: Kantarci)], R01 NS097495 (PI: Vemuri), R01 AG56366 (PI: Vemuri), U01 AG06786 (PI: Petersen/Mielke/Jack), P50 AG16574 (PI: Petersen), R37 AG11378 (PI: Jack), R01 AG41851 (PIs: Jack and Knopman)]; the Gerald and Henrietta Rauenhorst Foundation grant, Alzheimer's Drug Discovery Foundation (ADDF), the Alexander Family Alzheimer's Disease Research Professorship of the Mayo Foundation, Liston Award, Elsie and Marvin Dekelboum Family Foundation, Little Family Foundation, Mangurian Foundation, Ted Turner and Family Foundation, Schuler Foundation, Opus building National Institute of Health (grant C06 RR018898), and was made possible by Rochester Epidemiology Project (R01 AG34676). Elijah Mak is supported by the Alzheimer's Society Junior Research Fellowship (443 AS JF 18017), and an Alzheimer's Disease Research Developmental Project grant. John O'Brien is supported by the NIHR Cambridge Biomedical Research Centre (NIHR 203312). The authors thank AVID Radiopharmaceuticals, Inc., for the provision of the AV-1451 precursor, chemistry production, advice and oversight, and Food and Drug Administration regulatory cross-filing permission and documentation needed for this work. They particularly thank the patients and their family members for participating in this research.

Author contributions

E.M. contributed to conceptualization, methodology, writing—original draft, writing— review & editing, visualization. R.I.R. was responsible for data curation, formal analysis, methodology, writing—review & editing, and software. S.A P., A.M.F., and T.L. contributed to Writing—review & editing, visualization, methodology, formal analysis, and data curation. C.G.S. contributed to writing—review & editing, methodology, software. S.R., P.V., H.K.M., M.K.J, T.M., L.K.F., J.A.F., R.S., J.G.-R., D.T.J., H.B., E.K.St. L., D.S.K., V.K.R., D.W.D., N.R.G.-R., T.J.F., G.S.D., all contributed to writing—review &

editing and investigation. C.R.J., R.C.P., V.J.L., and B.F.B. were responsible for Writing—review & editing, resources, project administration. J.T.O'B., contributed to supervision, writing—review & editing. K.K. was responsible for writing—review & editing, supervision, resources, project administration, methodology, investigation, funding acquisition, and conceptualization.

Competing interests

E. Mak, R.I. Reid, S.A. Przybelski, A.M. Fought, and T.G. Lesnick report no disclosures relevant to the manuscript. C.G. Schwarz receives research support from the NIH. J. Graff-Radford serves on the editorial board for Neurology and receives research support from NIH. M.L. Senjem owns or has owned stock in medical-related companies, unrelated to the current work, within the past 36 months: Align Technology, Inc., Inovio Pharmaceuticals, Inc., Mesa Laboratories, Inc., Johnson and Johnson, LHC Group, Inc., Natus Medical Inc., and Varex Imaging Corporation. J.A. Fields reports no disclosures relevant to the manuscript. D.S. Knopman serves on a Data Safety Monitoring Board for the DIAN study, has served on a Data Safety Monitoring Board for a tau therapeutic for Biogen but received no personal compensation, is a site investigator in Biogen aducanumab trials, is an investigator in clinical trials sponsored by Lilly Pharmaceuticals and the University of Southern California, serves as a consultant for Samus Therapeutics, Roche, Magellan Health and Alzeca Biosciences but receives no personal compensation, and receives research support from the NIH. D.T. Jones reports no disclosures relevant to the manuscript. R. Savica reports no disclosures relevant to the manuscript. V.K. Ramanan receives research funding from the NIH and the Mangurian Foundation for Lewy Body disease research and has provided educational content for Medscape unrelated to this work. T. Ferman receives funding from the Mangurian Foundation for Lewy body research and NIH. NR Graff-Radford reports no disclosures relevant to the manuscript. V.J. Lowe serves as a consultant for Bayer Schering Pharma, Piramal Life Sciences, Life Molecular Imaging, Eisai Inc., AVID Radiopharmaceuticals, and Merck Research and receives research support from GE Healthcare, Siemens Molecular Imaging, AVID Radiopharmaceuticals, and the NIH (NIA, NCI). Clifford R. Jack Jr. is employed by Mayo Clinic. He receives grant funding from the National Institutes of Health (R37 AG011378, R01 AG041851), the Alexander family professorship and the GHR Foundation. Within the past 36 months, he served on a DSMB for Roche pro bono; no payments to the individual or institution were involved. He has received funding from the Alzheimer's Association for travel to scientific meetings. R.C. Petersen serves as a consultant for Roche, Inc., Merck, Inc., Biogen, Inc., Eisai, Inc., Genentech, Inc., and Nestle, Inc., served on a DSMB for Genentech, receives royalties from Oxford University Press and UpToDate, and receives NIH funding. B.F. Boeve has served as an investigator for clinical trials sponsored by Alector, Cognition Therapeutics, EIP Pharma, and Transposon. He serves on the Scientific Advisory Board of the Tau Consortium—funded by the Rainwater Charitable Foundation. He receives research support from NIH, the Mayo Clinic Dorothy and Harry T. Mangurian Jr. Lewy Body Dementia Program, the Little Family Foundation, and the Ted Turner and Family Foundation. E.K. Louis has no disclosures related to this work. He has served as a Co-Investigator on K. Kantarci research grant (DLB U01) and as a NAPS co-investigator. J.T. O'Brien. has no conflicts related to this study; unrelated to this work he has received honoraria for work as DSMB chair or member for TauRx, Axon, Eisai, has acted as a consultant for Roche, and has received research support from Alliance Medical and Merck. K. Kantarci consults for Biogen, receives research support from Avid Radiopharmaceuticals and Eli Lilly, and receives funding from NIH and Alzheimer's Drug Discovery Foundation. GS Day reports no competing interests directly relevant to this work. His research is supported by NIH (K23AG064029, U01AG057195, U01NS120901, U19AG032438). He serves as a consultant for Parabon Nanolabs Inc and as a Topic Editor (Dementia) for DynaMed (EBSCO). He is the co-Project PI for a clinical trial in anti-NMDAR encephalitis, which receives support from NINDS (U01NS120901) and Amgen Pharmaceuticals; and a consultant for Arialys Therapeutics. He has developed educational materials for Continuing Education Inc and Ionis Pharmaceutical. He owns stock in ANI pharmaceuticals. Dr. Day's institution has received support from Eli Lilly for development and participation in an educational event promoting early diagnosis of symptomatic Alzheimer disease, and in-kind contributions of radiotracer precursors for tau-PET neuroimaging in studies of memory and aging (via Avid Radiopharmaceuticals, a wholly owned subsidiary of Eli Lilly).

Additional information

Supplementary information The online version contains supplementary material available at https://doi.org/10.1038/s41531-025-00944-x.

Correspondence and requests for materials should be addressed to Elijah Mak.